Applied Nanoscience
https://doi.org/10.1007/s13204-023-02959-3

ORIGINAL ARTICLE

Optimizing silver nanowire synthesis: machine learning improves and predicts yield for a polyol, millifluidic flow reactor

Destiny F. Williams[1] · Nick Rahimi[2] · James E. Smay[3] · Shohreh Hemmati[1]

Received: 27 February 2023 / Accepted: 11 August 2023

Abstract
This study highlights optimizing polyol reaction conditions to produce 100% silver nanowire (AgNW) yields (AgNWs count/all nanostructure count) using a millifluidic flow reactor (MFR). AgNWs of uniform length and diameter offer potentially low-cost, transparent, and flexible conductors. MFRs produce AgNWs with superior uniformity, yield, and concentration due to the reduced dimensions of the reaction environment. A statistical design of experiments (DoE) considering polyol reaction temperature and the three reagent concentrations optimized the process. The AgNWs are characterized by scanning electron microscopy (SEM) to calculate the yield of AgNWs per reaction. After completing the DoE, calculated yields are put into Minitab statistical software for analysis. Minitab discovered the optimal reaction conditions to be $T = 170$ °C, $[AgNO_3] = 0.177$ M, $[CuCl_2] = 6.05$ mM, and [PVP] = 0.224 M, with an R^2 value of 85%. Results of the DoE were imported into supervised decision tree (DT) and random forest (RF) machine learning (ML) algorithms. The DT and RF predicted yields of AgNWs given reaction temperature and reagent concentrations with 96.9% and 97.5% accuracy, respectively. The optimal polyol reaction conditions synthesized 100% AgNW yield with average concentrations of 16 mg/mL, lengths of 32 µm ($\sigma \pm 3.5$ µm), diameters of 68 nm ($\sigma \pm 12$ nm), and aspect ratios of 475.

Keywords Silver nanowires · Polyol · Millifluidic flow reactor · Continuous flow reactor · Design of experiment · Machine learning

Introduction

One-dimensional (1D) silver nanowires (AgNWs), with high aspect ratios, optical transparency, photoluminescence, and high electrical and thermal conductivity are leading candidates for future nanomaterial applications in nanoelectronics, nanophotonics, optoelectronics, and micromechanics (Luu et al. 2011; Hemmati et al. 2015). These include smart sensors (Hemmati et al. 2016; Lee et al. 2016; R et al. 2015), wearable electronics (Kwon et al. 2018; Huang and Zhu 2019), catalysts (Kostowskyj et al. 2008), energy harvesting devices (Liang et al. 2019), and various other types of stretchable sensors (Choi et al. 2015; Liang et al. 2014; Miller et al. 2013; Kumar et al. 2021). AgNWs are commonly synthesized using templates or using wet-chemical techniques like hydrothermal, solvothermal, and polyol-based synthesis techniques that heretofore require a costly and time-consuming separation and purification step (Kumar et al. 2021).

There are two major types of template syntheses for AgNWs including soft and hard templates. Typical hard template examples include nanoporous membranes and carbon nanotubes, while typical examples of soft templates include micelles, surfactants, and various polymers (Zhang et al. 2017). In template-based syntheses, the AgNWs are grown on specific templates in the presence of reagents undergoing either electrochemical (Dalchiele et al. 2007),

✉ Shohreh Hemmati
shohreh.hemmati@okstate.edu

Destiny F. Williams
destiny.f.williams@okstate.edu

Nick Rahimi
nick.rahimi@usm.edu

James E. Smay
jim.smay@okstate.edu

[1] School of Chemical Engineering, Oklahoma State University, Stillwater, OK, USA

[2] School of Computing Sciences and Computer Engineering, University of Southern Mississippi, Hattiesburg, MS, USA

[3] School of Material Sciences Engineering, Oklahoma State University, Tulsa, OK, USA

Published online: 31 August 2023

chemical reduction (Malandrino et al. 2004), or irradiation (Hong et al. 2015) processes to produce silver atoms that propagate nanowire growth. The advantage of hard template syntheses is the ability to synthesize highly ordered, well-defined morphologies, but the major disadvantage is the complex removal process of the AgNWs from the templates. Soft templates were introduced to overcome the issues associated with the nanomaterial removal process, but the disadvantages changed from a difficult removal process to low amounts of AgNWs produced, polycrystallinity, low aspect ratios, and irregular morphologies (Zhang et al. 2017).

Two common wet-chemical techniques are hydrothermal (Xu et al. 2006) and solvothermal (Chen et al. 2011). Each of these processes include mixing reagents in a reaction vessel, placing the reactor into a furnace, allowing time for the reaction to proceed, cooling the reaction solution, and then separating and washing the nanowires from the reaction solution. Advantages of using one of these methods include using greener solvents (water in hydrothermal processes) and being able to seal the reaction vessel to allow for large arrays of reaction temperatures. A disadvantage of these techniques is that organic solvents are used instead of water (in solvothermal processes) and both methods require detailed separation processes for the nanowires (Zou et al. 2006). Despite these challenges, wet-chemical techniques can be more readily implemented than template-based methods.

The polyol wet-chemical technique is a simple, cost-effective way to synthesize AgNWs with uniform diameters and lengths. Polyol synthesis requires a glycol as the solvent and reducing agent, a metal precursor, polyvinylpyrrolidone (PVP) as the capping agent, and a salt mediator to scavenge oxygen, as well as slowly release silver ions into solution during the reaction (Hemmati et al. 2017). Cao et al. used a modified polyol method to synthesize AgNWs using a batch reactor. Silver nitrate, ethylene glycol (EG), and PVP were used as the metal precursor, reducing agent, and capping agent, respectively. Sodium chloride and sodium bromide were used as the halide mediators for the modified polyol process. The AgNWs formed in this study had average lengths of 24 µm with 70 nm average diameters (Cao et al. 2020). Nekahi et al. produced sharp-end and round-end AgNWs in a batch reactor using another modified polyol process. Silver nitrate, EG, and PVP were used as the metal precursor, reducing agent, and capping agent, respectively. In this study, a salt mediator was not used in the polyol reaction. The authors controlled the silver ion concentration by adding the reagent solutions into the reaction flask drop wise over 8 min. The AgNWs synthesized in this study reported average lengths of 28 µm and average diameters of 215 nm (Nekahi and Fatmesari 2016). Zhao et al. synthesized AgNWs using a traditional polyol process in a batch reactor. Silver nitrate, EG, PVP, and ferric chloride were used as the metal precursor, reducing agent, capping agent, and salt mediator, respectively. They investigated the effects of adding different amounts of ferric chloride and PVP to produce long and uniform AgNWs. The authors reported a maximum aspect ratio of 570 for the AgNWs (Zhao and Qu 2018).

Batch processes are known for low AgNW yields, low aspect ratio AgNWs, and irregular morphologies (Hemmati et al. 2017). In order for a process to be eligible for scale up, it must demonstrate control over the morphologies synthesized and be reproducible for quality assurance. Convective mass and heat transfer dominate in batch reactors due to turbulent flow conditions (Roberts et al. 2019). Nanowires from batch reactions are unreproducible due to mass and thermal transport properties changing with respect to volume (Bertuit and Abou-Hassan 2022). As reaction volume gets larger, it is more difficult to achieve uniform mixing, so custom impeller geometries must be configured (Roberts et al. 2019).

Continuous flow reactors operating at low Reynolds (Re) allow diffusion dominated heat and mass transport throughout the reaction and the nanowires grow in the well-organized streamlines of laminar flow. In this work, a combination of laminar flow, and a coiled reactor tube results in secondary flow called Dean vortices that aid mixing of the reagents throughout the synthesis. Dean vortices create a secondary, transverse flow to the bulk fluid's flow which produces transverse drag on the NWs being synthesized. Even at low Deans numbers, the drag from the secondary flow allows for long AgNWs to be synthesized. When considering scale out, or identical flow reactors in parallel, the dimensionless numbers that are dependent on reactor size and configuration remain constant which allows for scalable repeatable synthesis. When considering a technique with potential for scale out, continuous flow syntheses show great promise (Bertuit et al. 2022; Kinhal et al. 2019).

Gottesman et al. synthesized AgNWs in a millifluidic flow reactor (MFR) utilizing the polyol synthesis. The authors used polytetrafluoroethylene (PTFE) tubing placed inside of a split furnace heated to 198 °C. Silver nitrate, EG, and PVP were used as the metal precursor, reducing agent, and capping agent, respectively. A salt mediator was not used in this process. They reported AgNWs with average lengths of 10 µm and diameters of 71 nm (Gottesman et al. 2012). Hemmati et al. synthesized AgNWs in a MFR using the polyol process. The authors used PTFE tubing submerged in an isothermal bath of silicone oil at reaction temperatures of 120 °C, 130 °C, 140 °C, or 150 °C. Silver nitrate, EG, PVP, and copper chloride were used as the metal precursor, reducing agent, capping agent, and salt mediator, respectively. A proposed reaction mechanism by the authors is outlined in Fig. 1. They reported synthesizing AgNWs at temperatures as low as 130 °C (Hemmati et al. 2017).

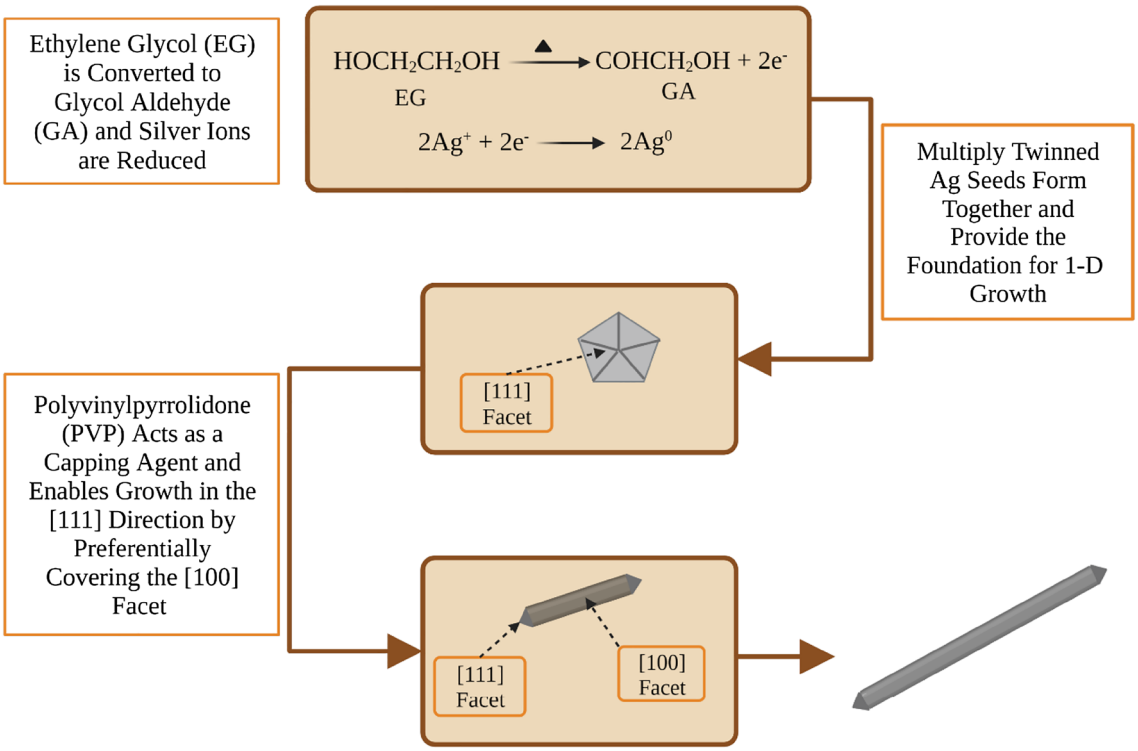

Fig. 1 Proposed reaction mechanism for the polyol process. In a polyol synthesis of AgNWs, solutions of silver nitrate, PVP, and copper chloride are prepared in EG. Silver nitrate dissociates in solution due to ionic bonding properties. When exposed to heat, the EG converts to glycol aldehyde (GA), and acts as a reducing agent. The GA reduces the silver ions which allows nucleation and growth into multiply twinned silver seeds. PVP is used as a stabilizing and capping agent because it preferentially adsorbs onto the [100] facets which promotes one-dimensional growth (Hemmati et al. 2017) (image created with BioRender)

Lau et al. synthesized AgNWs in a continuous flow reactor using the polyol method. A 10 mL perfluoroalkoxy (PFA) reaction coil placed on a heater set to 130 °C was used for the synthesis. Silver nitrate, EG, PVP, and sodium chloride were used as the metal precursor, reducing agent, capping agent, and salt mediator, respectively. The authors reported AgNWs with average lengths of 36 µm and average diameters of 95 nm (Sheng Lau et al. 2019).

Replicating the millifluidic polyol process reported by Hemmati et al. (Hemmati et al. 2017), repeatedly produced a small amount of silver nanoparticles (AgNPs) along with the AgNWs. To help address this problem, the optimal reaction conditions of a batch study by Hemmati et al. (Hemmati and Barkey 2017) were applied to the MFR. The authors performed a parametric study with reaction temperature, silver nitrate concentration and sonication time, salt mediator type and copper chloride concentration, and PVP concentration and molecular weight to understand the impact of each factor. The outcome was that the reactions were heavily impacted by changes in reaction temperature, [$AgNO_3$], sonication time, salt mediator type and concentration, and [PVP] and PVP molecular weight. To refine the optimal reaction conditions, a design of experiments (DoE) was created using the statistical software JMP Pro. The authors found the optimum reaction conditions to be $T = 158$ °C, [$AgNO_3$] = 0.102 M, [PVP] = 0.124 M, and [$CuCl_2$] = 5.16 mM (Hemmati and Barkey 2017). Applying the batch optimal conditions improved the yield of AgNWs produced per millifluidic reaction but was still not at 100%. Under these conditions, the average AgNW concentration ([AgNW]) calculated was 5 mg/mL.

In machine learning (ML), a computer imports data and applies statistical science to learn directly from the data to make future predictions in the algorithm (Anuoluwa Bamidele et al. 2022). Given a quality training set involving myriad variables that impact the desired outcome, ML can be used to discover new materials (Li et al. 2020) and optimize known materials (Mahalle et al. 2019). In this study, the material is AgNWs, and the application of ML is to use data from the DoE to train a model to accurately predict AgNW yields given varying input parameters. The vast capabilities of ML lie within three major categories of algorithms such as reinforcement learning (Pareek et al. 2021), supervised ML (Ji et al. 2022), and unsupervised ML (Lv and Chen 2022). Reinforcement learning aims to find optimal relationships or predict actions to maximize

cumulative reward for the selected material properties. After learning from labeled data, supervised ML finds the hidden relationship between known inputs and unknown outputs while unsupervised ML learns from unlabeled data. While ML is a new and exciting area in nanomaterials science, there are certain nuances or issues associated with using these algorithms. The most common nuances include underrepresented classes, descriptor selection, underfitting, overfitting, model interpretability, and feature extraction. Selecting the appropriate type of algorithm and descriptor for the material helps researchers manage these nuances (Anuoluwa Bamidele et al. 2022).

When considering an appropriate ML algorithm for nanomaterial synthesis and optimization, supervised ML algorithms are commonly used. Supervised ML algorithms encompass several ML algorithms such as regression, decision tree (DT), random forest (RF), support vector machine (SVM), naïve Bayes, k-nearest neighbor (KNN), and artificial neural networks (ANN). When considering the best supervised algorithm for nanomaterial synthesis optimization, DT and RF are commonly applied (Nathanael et al. 2023; Ono et al. 2023; Kenry 2023). Advantages of DT algorithms include clear visualization, handling of missing data easily, scaling data is not necessary, requires less data and processing efforts, data normalization is unnecessary, and the models are intuitive. The advantages of RF algorithms are that they handle large data sets, outliers have a negligible impact, they handle missing data easily, and they easily estimate and reduce error. Disadvantages of DT algorithms include taking a long time to train, requiring expensive computations, not being able to predict continuous values, not being able to handle large data sets, and susceptible to overfitting. The disadvantages for RF algorithms are that they are not easy to control, and regression predictions can be inaccurate. Considering the advantages, DT and RF algorithms are reliable methods for synthesis and optimization of nanomaterials (Saraee et al. 2017; Tashkhourian et al. 2011; Anuoluwa Bamidele et al. 2022).

Decision tree algorithms import the data and then divide it into smaller pieces until a pattern emerges. These patterns form a flow pattern which resembles a tree as seen in Fig. 2. Each node indicates where a decision has been made based on a parameter, and when the nodes split that indicates multiple decision possibilities. After several nodes have split and subdivided, the flow path is completed with a final node. A terminal node indicates when the division of data stops, and the final nodes share the same conclusions (Galvão et al. 2020).

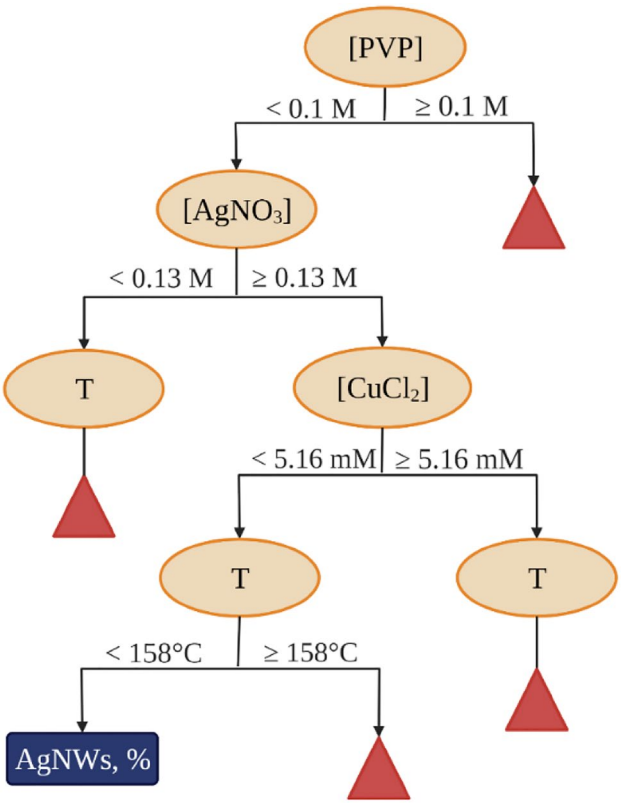

Fig. 2 An example of a DT algorithm for AgNW polyol synthesis where the oval nodes represent parameters and the numbers on the branches represent high and low values of the parameters (triangles represent other nodes in the DT) (Galvão et al. 2020) (image created with BioRender)

Random forest algorithms utilize a method called bagging which uses the outcome of several decision tree algorithms to make predictions as seen in Fig. 3. Specifically, RF algorithms utilize sample and property bagging to reduce the number of properties which creates several different DT algorithms. Relying on the anticipated outcome allows RF algorithms to reduce the number of properties based on the outcome as the DTs are made. All the DT outcomes are then statistically analyzed to produce a final prediction (Galvão et al. 2020).

Gholizadeh et al. focused on applying a RF algorithm to predict the viscosities of Newtonian nanofluids. The authors identified the input parameters as solid volume fraction, viscosity of the base fluid, temperature, density of nanoparticle, and nanoparticle size, and trained the RF algorithm on 2890 datasets from 50 references. To assess the accuracy of the RF model, the model was compared to a multilayer perceptron (MLP) model and a support vector regression (SVR) model.

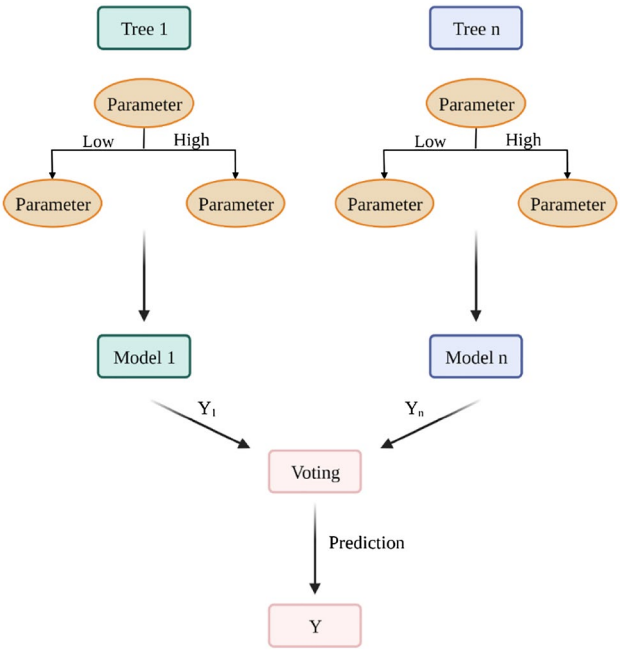

Fig. 3 An example of a random forest machine learning algorithm for AgNW polyol synthesis that utilizes bagging to create several decision tree outcomes that can then be statistically analyzed to make a prediction (Galvão et al. 2020) (image created with BioRender)

When comparing the R^2 values, the RF model had 98.9% accuracy while the MLP and SVR models had 91.5% and 94.1% accuracies, respectively (Gholizadeh et al. 2020). Han et al. optimized, accelerated, and predicted the quantum yield (QY) of carbon dots (CDs) using a regression DT algorithm. Volume of the precursor, mass of the precursor, time, temperature, and ramp rate were identified as the important input parameters. The authors used 391 sets of data to train the DT algorithm and found that CDs with strong green emission with QYs up to 39.3% could be obtained from the DT model and then experimentally verified (Han et al. 2020). Liu et al. studied the cytotoxicity of photosynthesis synthesized silver nanoparticles (AgNPs). The extraction/solvent, exposure dose, particle size, exposure time, normal/cancerous cells, and zeta potential were classified as the important factors in predicting cytotoxicity using DT and RF ML algorithms, and 690 data sets were used to train the models. To verify the models, the authors compared the accuracy of published works to the DT and RF algorithms used. A baseline prediction accuracy for published data is 55.6% and the authors were able to model cytotoxicity using a RF model with 90% accuracy (Liu et al. 2021).

This study used the findings from the previous optimization by Hemmati et al. (Hemmati and Barkey 2017) to create a design of experiments (DoE) using the Minitab statistical software aimed to optimize the polyol reaction conditions for the millifluidic synthesis of AgNWs. In addition, the data obtained from the DoE reactions were input to a linear regression model

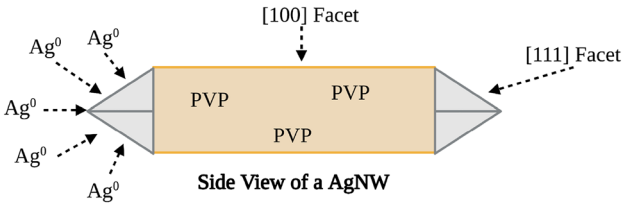

Fig. 4 The proposed mechanism shows PVP (in orange) preferentially depositing on the [100] facets of the multiply twinned Ag seeds which allows the Ag atoms in solution to preferentially deposit on the [111] facets located at the ends of the AgNWs (Sun et al. 2003) (image created with BioRender)

software and imported into supervised ML algorithms aimed to calculate or predict the yield of AgNWs given reaction temperature and reagent concentrations.

Results and discussion

Design of experiments

A DoE was created using the Minitab software with parameters of reaction temperature and reagent concentrations of silver nitrate, copper chloride, and PVP. A central composite, response surface design was selected to evaluate the DoE in lieu of the Box–Behnken design. Central composite designs are a factorial design with center points supplemented by a group of axial points that allow for more accurate optimization. Response surface designs can more accurately optimize a process because a response surface factorial design includes the addition of the quadratic term that allows for more accurate modeling in the response of the DoE. Box–Behnken designs are response surface designs that do not contain an embedded factorial design, so these designs only account for one value above and below (± 1.0) the base parameters (Support 2022a). The central composite, response surface design accounts for two values above and below (± 1.0 and ± 1.68179) the base parameters for a more thorough, conclusive response that searches beyond the base parameters (Support 2022b). The DoE is designed to find a response that optimizes reaction parameters to produce 100% yield of AgNW using a MFR. The parameters, based on the findings of Hemmati et al., are reaction temperature, silver nitrate concentration, copper chloride concentration, and PVP concentration (Hemmati and Barkey 2017).

Reaction temperature is vital for converting EG to glycolaldehyde (GA) so that silver atoms can undergo homogenous nucleation. The ratio of PVP to silver nitrate heavily impacts the morphology of synthesized AgNWs in polyol syntheses. When the concentration of silver nitrate is too

high, passivation of the [100] facets on the Ag seeds is insufficient and growth occurs on both [100] and [111] facets. Growth on [111] facets encourage AgNP formation in lieu of the desired AgNW morphology. When the concentration of silver nitrate is too low, the excess PVP covers all surfaces, including [100] facets of the Ag seeds and prevents 1D AgNW growth. A proposed mechanism of PVP acting as a capping agent is shown in Fig. 4 (Coskun et al. 2011).

Sonicating the silver nitrate solutions for 5–6 min minimized the by-product nanoparticles and allowed for longer wires to form. In the presence of heat, oxygen in solution adsorbs onto the surface of the silver seeds. Adsorbed oxygen on the surface during the nucleation and growth steps can cover different facets on the silver seeds and prevent 1D growth. To minimize this adverse adsorption, copper chloride was used as the salt mediator. The copper (II) ions get reduced by EG, once EG has converted to GA, and then go on to react with the adsorbed oxygen to remove it from the surface of the silver seeds. This process allows the Cu^{+} ions to convert back to Cu^{2+} ions to be reduced and used again for scavenging oxygen as seen in Fig. 5 (Hemmati and Barkey 2017).

In the presence of heat, the silver ions will form an ionic bond with the chloride ions. This compound dissociates throughout the nucleation and growth phases, which allows for silver ions to be released slowly into the reaction solution to undergo reduction. This functionality of the salt mediator allows for Ag to be slowly added to the multiply twinned silver seeds. The concentration and molecular weight of PVP are critical in controlling growth and morphology of the silver seeds into AgNWs. PVP with a molecular weight of 55,000 was found to be the optimal molecular weight because it easily covered the surface of silver seeds due to its low steric effect and preferentially capped the [100] facets of the silver seeds (Hemmati and Barkey 2017).

Table 1 Base, low, and high parameter values for the DoE

Value	T, °C	$[AgNO_3]$, M	$[CuCl_2]$, mM	[PVP], M
− 1.7	144	0.0019	3.1614	0.02435
−	151	0.0519	4.1614	0.07435
0	158	0.1019	5.1614	0.12435
+	165	0.1519	6.1614	0.17435
+1.7	172	0.2019	7.1614	0.22435

For baseline conditions, the findings from Hemmati et al. were applied. The baseline conditions are $T = 158$ °C, $[AgNO_3] = 0.102$ M, $[PVP] = 0.124$ M, and $[CuCl_2] = 5.16$ mM as seen in Table 1 (Hemmati and Barkey 2017). Based on four input parameters, the DoE consisted of 31 total experiments as shown in Table 2.

The SEM images taken of the 31 DoE reactions can be seen in Fig. 6.

Minitab linear regression model

Upon the completion and analysis of the 31 DoE reactions, the data were put into the Minitab software and analyzed using a response surface design. Once the software analyzed the data, significant factors could be identified by comparing the *p*-value calculated by the software to the standard α term in the software. Minitab assigns α *a* value of 0.05, so if a parameter has a *p*-value less than α, the parameter is considered statistically significant to the process. In Table 3, the parameters, variables, and *p*-values are listed. A pareto chart in Fig. 7 is used to graphically depict the data seen in Table 3. Based on Fig. 7 and Table 3, only silver nitrate concentration (B), PVP concentration (D), and

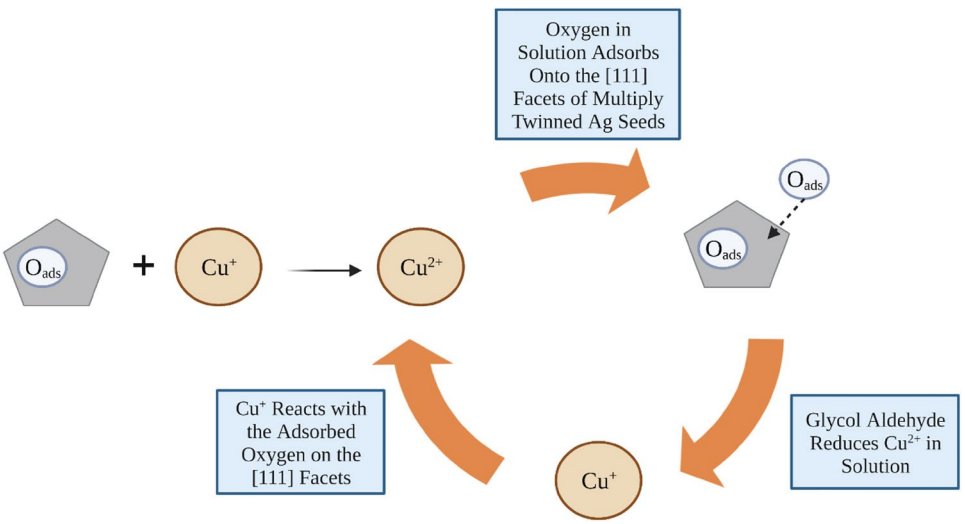

Fig. 5 Copper chloride dissociates in EG due to ionic bonding properties, copper (II) is reduced to copper (I) by glycol aldehyde (GA), oxygen adsorbs onto the surface of multiply twinned silver seeds, copper (I) scavenges the adsorbed oxygen, gains an electron, and converts back to copper (II), and finally copper (II) is reduced again by GA and the process repeats (Korte et al. 2008) (image created with BioRender)

Table 2 DoE reaction conditions for 31 polyol AgNW syntheses

DoE	Parameters	T, °C	$[AgNO_3]$, M	$[CuCl_2]$, mM	[PVP], M
1	− 1.7 0 0 0	144	0.1019	5.1614	0.12435
2	− − + +	151	0.0519	6.1614	0.17435
3	− + − −	151	0.1519	4.1614	0.07435
4	– − + -	151	0.0519	6.1614	0.07435
5	− + + +	151	0.1519	6.1614	0.17435
6	− + − +	151	0.1519	4.1614	0.17435
7	− + + −	151	0.1519	6.1614	0.07435
8	− − − −	151	0.0519	4.1614	0.07435
9	− − − +	151	0.0519	4.1614	0.17435
10	0 − 1.7 0 0	158	0.0019	5.1614	0.12435
11	0 0 + 1.7 0	158	0.1019	7.1614	0.12435
12	0 0 0 − 1.7	158	0.1019	5.1614	0.02435
13	0 0 − 1.7 0	158	0.1019	3.1614	0.12435
14	0 0 0 0	158	0.1019	5.1614	0.12435
15	0 0 0 0	158	0.1019	5.1614	0.12435
16	0 + 1.7 0 0	158	0.2019	5.1614	0.12435
17	0 0 0 0	158	0.1019	5.1614	0.12435
18	0 0 0 0	158	0.1019	5.1614	0.12435
19	0 0 0 + 1.7	158	0.1019	5.1614	0.22435
20	0 0 0 0	158	0.1019	5.1614	0.12435
21	0 0 0 0	158	0.1019	5.1614	0.12435
22	0 0 0 0	158	0.1019	5.1614	0.12435
23	+ + − −	165	0.1519	4.1614	0.07435
24	+ − + +	165	0.0519	6.1614	0.17435
25	+ − − +	165	0.0519	4.1614	0.17435
26	+ + − +	165	0.1519	4.1614	0.17435
27	+ + + −	165	0.1519	6.1614	0.07435
28	+ − − + −	165	0.0519	6.1614	0.07435
29	+ − − −	165	0.0519	4.1614	0.07435
30	+ + + +	165	0.1519	6.1614	0.17435
31	+ 1.7 0 0 0	172	0.1019	5.1614	0.12435

their self-interactions (BB and DD) parameters should be considered significant to the process. When this is the case, a model reduction is usually required to properly fit a model.

The previously discussed impact of reaction temperature and copper chloride concentration (Hemmati and Barkey 2017), as well as the experimental results from this study (Fig. 6) exhibit a dependence on all four parameters. To investigate whether these factors were significant, the mean of yield (average percentage of AgNWs in each reaction for each parameter) for each factor is represented in Fig. 8. When analyzing a main effects plot, a linear mean of yield line implies that the effect of a parameter is insignificant, but a non-linear mean of yield line implies an effect of a parameter is significant. The steepness of the non-linear line implies how large the parameter effect is. Considering the findings from Hemmati et al., experimental evidence from this study, and results from the mean yield plot generated by Minitab, all parameters were considered when fitting the model.

A regression model was performed and an R^2 value of 85% was calculated by the Minitab software. The model determined by the Minitab software to predict AgNW yield given temperatures and reagent concentrations is shown in Eq. 1:

$$\begin{aligned}\%\text{AgNWs} = {} & -2821 + 32.2 \bullet \mathrm{T} - 842 \cdot \left[AgNO_3\right] + 171 \cdot \left[CuCl_2\right] \\ & - 1357 \cdot [\mathrm{PVP}] - 0.0991 \cdot \mathrm{T}^2 - 5169 \cdot \left[AgNO_3\right]^2 \\ & - 5.92 \cdot \left[CuCl_2\right]^2 - 4369 \cdot [\mathrm{PVP}]^2 + 16.9 \cdot \mathrm{T} \cdot \left[AgNO_3\right] \\ & - 0.736 \cdot \mathrm{T} \cdot \left[CuCl_2\right] + 12.8 \cdot \mathrm{T} \cdot [\mathrm{PVP}] \\ & - 125.4 \cdot \left[AgNO_3\right] \cdot \left[CuCl_2\right] + 2047 \cdot \left[AgNO_3\right] \cdot [\mathrm{PVP}] \\ & + 107.7 \cdot \left[CuCl_2\right] \cdot [\mathrm{PVP}]\end{aligned} \tag{1}$$

where the units for temperature, silver nitrate concentration, copper chloride concentration, and PVP are degrees Celsius, molar, millimolar, and molar, respectively. The Minitab regression model and the experimental data are graphed in Fig. 9 for each DoE reaction.

When the R^2 value is low, Minitab suggests a model reduction (removing statistically insignificant parameters) to try to raise the R^2 value. A model reduction was performed to only include the statistically significant variables found in Fig. 7 and a model and R^2 value was calculated by the software. The model reduction produced an even lower R^2 value equal to 68%. Several variations of model reductions were performed, but none produced an R^2 value above 85%. It was determined that all four variables are significant and necessary to properly model the data.

Looking more closely at the data in Fig. 9 for DoE 26, the regression model shows that the yield for AgNWs is predicted to be greater than 100% for the given reaction conditions. While this point stands out because it exceeds 100%, there are a few other points, DoE 2, 3, 25, 27, 28, and 29, that exhibit an extreme overshoot or undershoot for prediction. Figure 6 shows that these reaction conditions promote AgNP formation because the ratio of [PVP] and $[CuCl_2]$ were either too low or too high for the $[Ag^+]$ in solution. It is experimentally anticipated for AgNPs to form when the [PVP] and $[CuCl_2]$ concentrations are too high or too low in the reaction solution and it is verified from the reaction product images in Fig. 6. The results from this model have proved that linear regression models are not a viable way to predict the yield of AgNWs. A model capable of accounting for and noting the sensitive relationship between the reagents during nucleation and growth phases of AgNW formation is required to adequately model and predict AgNW yields.

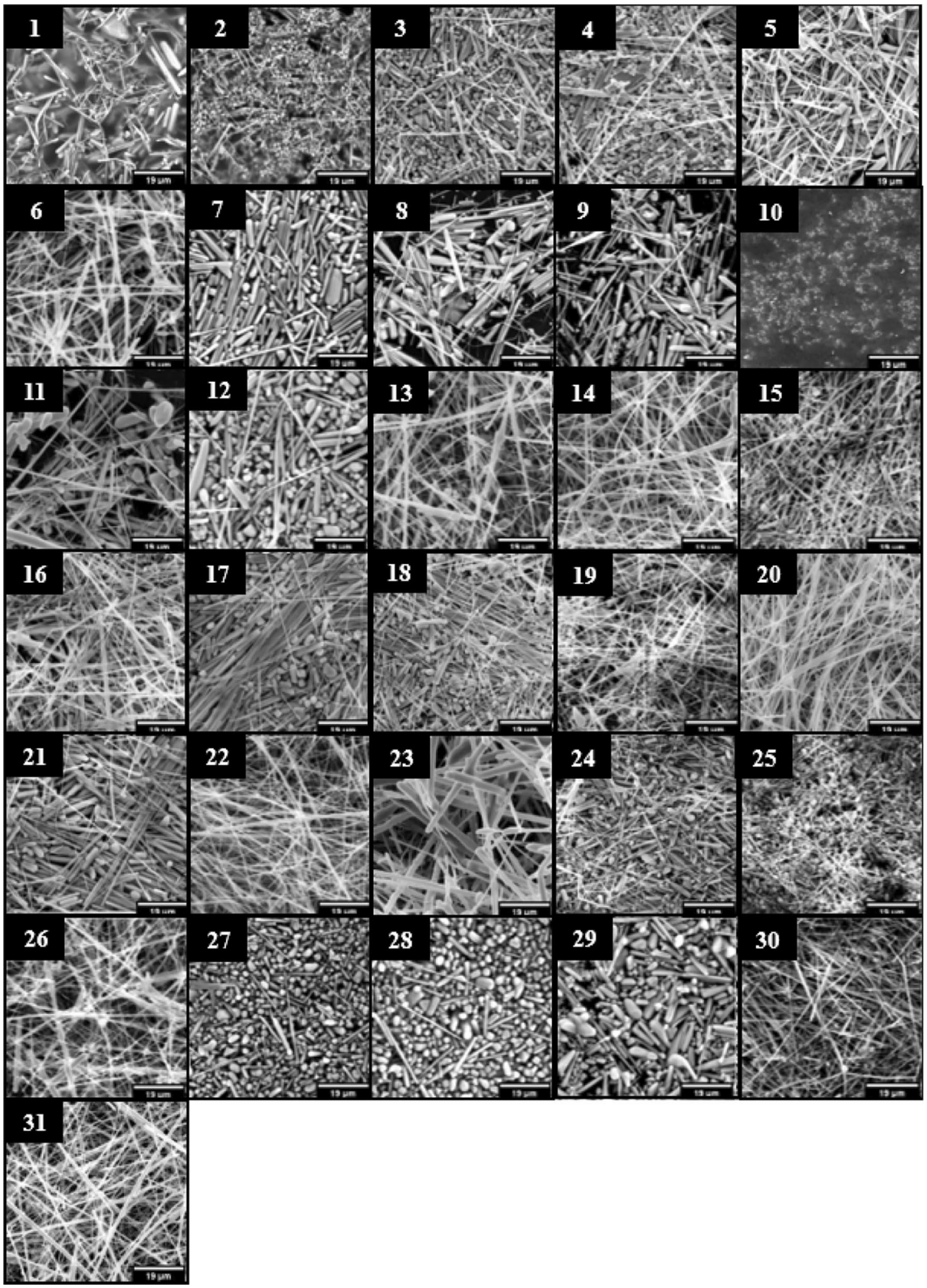

Fig. 6 SEM images of silver nanostructures synthesized at different reaction conditions (reaction conditions correspond to the values found in Table 2) (scale bars: 19 μm)

Table 3 Table of *p*-values assigned by Minitab to help identify significant parameters

Parameter	Parameter variable	*P*-value
T	A	0.497
$[AgNO_3]$	B	0
$[CuCl_2]$	C	0.139
[PVP]	D	0
T*T	AA	0.164
$[AgNO_3]$*$[AgNO_3]$	BB	0.001
$[CuCl_2]$*$[CuCl_2]$	CC	0.094
[PVP]*[PVP]	DD	0.005
T*$[AgNO_3]$	AB	0.203
T*$[CuCl_2]$	AC	0.264
T*[PVP]	AD	0.328
$[AgNO_3]$*$[CuCl_2]$	BC	0.178
$[AgNO_3]$*[PVP]	BD	0.267
$[CuCl_2]$*[PVP]	CD	0.244

Machine learning algorithms

To conduct the experiment, the RF and DT algorithms in Python were utilized, leveraging libraries such as pandas and scikit-learn for data manipulation, executing the machine learning algorithms, and evaluating metrics. To test the effectiveness of the model and assess feature correlation, the cross-validation was performed. This technique enables estimation of the performance of the model on unseen data and gain insights into its generalization capabilities. To train the algorithms, 31 data sets each containing 3 data points each (93 total) from the DoE reactions, were used in DT and RF ML algorithms. The selected parameters for the algorithms are $[AgNO_3]$, [PVP], $[CuCl_2]$, reaction temperature, and predicted yield of AgNWs. When applying the DT algorithm to the data, the depth of the tree was set to unlimited, and the test mode was a fivefold cross-validation. The DT ended up having 45 nodes corresponding to an R^2 value of 96.9%. For the RF algorithm, bagging with 100 iterations and base learner were applied to the data which produced an R^2 value of 97.5%. Both ML algorithms improved prediction accuracy over the Minitab regression model and each model took less than 1 s to build.

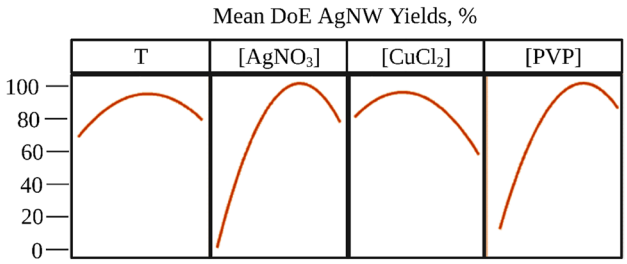

Fig. 8 A main effects plots shows the mean AgNW yield for each parameter of each DoE reaction

Minitab response optimization

After modeling the data, a response optimization was performed in the Minitab software. The response optimization graphed the AgNW yields across the minimum and maximum values for each parameter considered as seen in Fig. 10. Considering where the graphed parameters intersected the 100% yield threshold, the software produced the reaction conditions of $T = 170$ °C, $[AgNO_3] = 0.177$ M, $[CuCl_2] = 6.05$ mM, and [PVP] = 0.224 M.

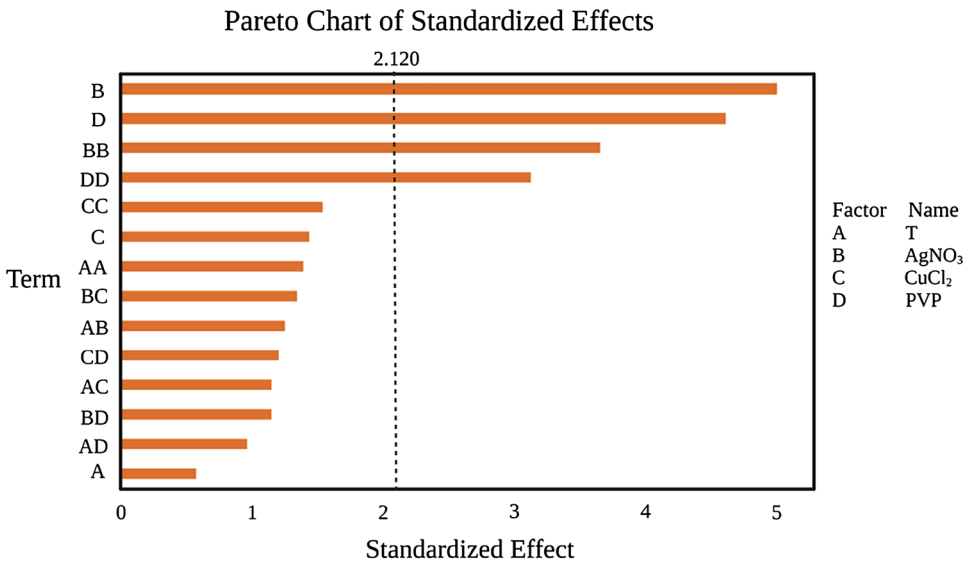

Fig. 7 A Pareto chart is used to determine the magnitude and the importance of the parameters by analyzing the yield response of the reaction parameters; the bars that extend past the dotted reference line are considered statistically significant (image created with BioRender)

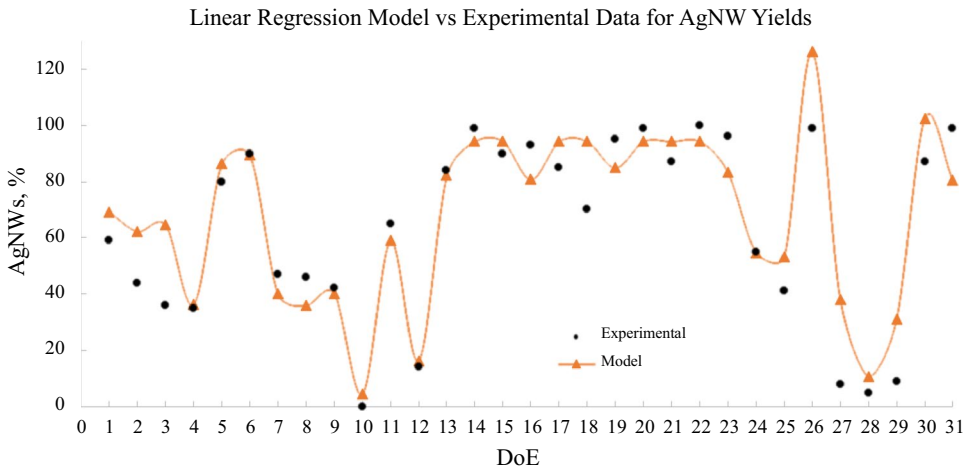

Fig. 9 For each DoE reaction, the experimental data and the model prediction were graphed (reaction conditions correspond to the values found in Table 2)

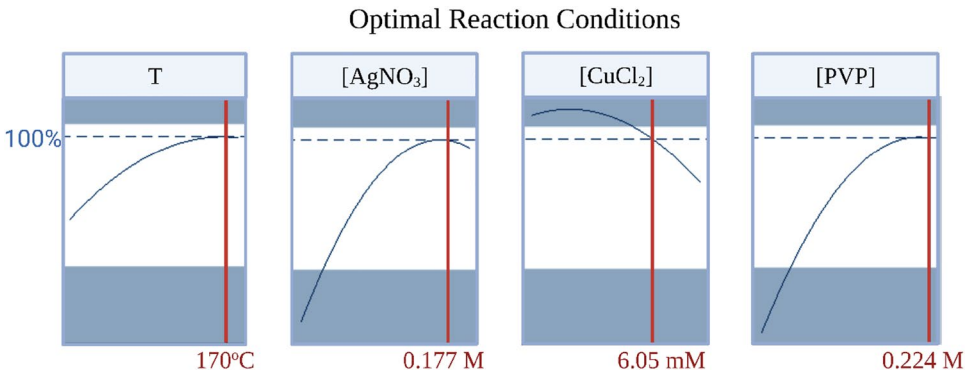

Fig. 10 Optimized reaction conditions based on the DoE analysis for reaction temperature and reagent concentrations is shown

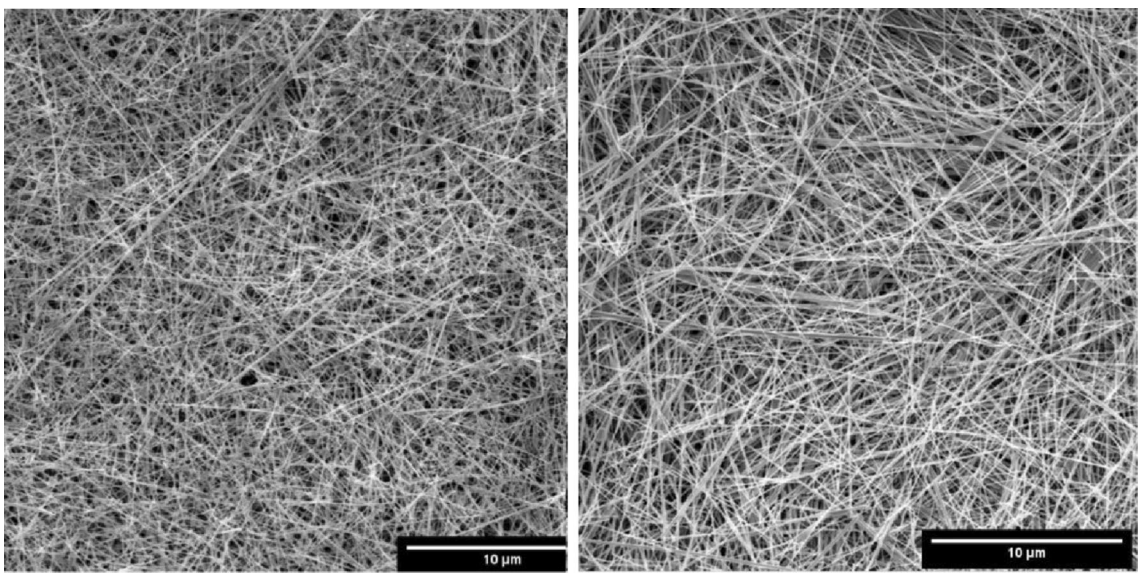

Fig. 11 SEM images of two different reactions conducted at optimal conditions (OC) with 100% AgNW yields (scale bars: 10 µm)

Two separate reactions were conducted and repeated at the optimal reaction conditions to establish reproducibility of the synthesis. The AgNWs were synthesized, washed, prepared, characterized, and analyzed in the same manner as the 31 DoE reactions in Table 2. Figure 11 shows two SEM images taken from the two identical optimal reactions. After analysis, it was determined that each reaction yielded 100% AgNWs. In addition, 45 AgNWs were measured using SEM and ImageJ software to obtain the average length and diameter to calculate the aspect ratio. The optimal reaction conditions produced 100% AgNWs with average concentration of 16 mg/mL, lengths of 32 µm ($\sigma \pm 3.5$ µm), diameters of 68 nm ($\sigma \pm 12$ nm), and aspect ratio of 475. The aspect ratio is high compared to other reported values for the continuous polyol synthesis of AgNWs (Gottesman et al. 2012; Sheng Lau et al. 2019).

Experimental

AgNW synthesis

The AgNWs were synthesized using a polyol method in a continuous, MFR. The reactor was assembled by coiling and submerging PTFE tubing in a silicone oil bath as shown in Fig. 12.

The length of tubing was calculated to achieve a residence time of 90 min with a flow rate of 40 µL/min (Hemmati et al. 2017). To control the flowrate, a syringe pump was used for reagent addition. Reagent solutions of copper chloride, PVP, and silver nitrate were prepared in EG according to the concentrations found in Table 2 for each DoE reaction. Once the reagents were prepared, PVP and copper chloride were sonicated until homogeneously mixed, while silver nitrate was sonicated for 6 min (Hemmati and Barkey 2017). After sonication, 60 µL of copper chloride was added to both PVP and silver nitrate solutions and mixed (Hemmati et al. 2017). The PVP/copper chloride and silver nitrate/copper chloride solutions were then loaded into 5 mL plastic syringes and connected to the reactor tubing. The synthesized AgNWs were collected into a Falcon tube collection flask at the outlet of the reactor. Once the samples were cooled to room temperature, they were washed and centrifuged at 3000 RPM for 30 min, once with acetone and then twice more with deionized water (DIW). The samples were then stored in DIW for further characterization.

Materials

The MFR was comprised of a pump (Chemyx, F100X), plastic syringes (Brandzig, 5 mL, Leur Slip), 1.5 mm I.D. polytetrafluoroethylene (PTFE) tubing, 1.5 mm I.D. polypropylene, t-joint connectors, a hot plate, and a Falcon tube collection flask. Silicone oil (Fisher, 200553), Copper (II) Chloride ($CuCl_2$, Sigma-Aldrich, 203149, 99%), Polyvinylpyrrolidone (PVP, Sigma-Aldrich, 856568, Avg. MW: 55,000), Silver Nitrate ($AgNO_3$, Sigma-Aldrich, 209139, $\geq$ 99%), Ethylene Glycol (EG anhydrous, Sigma-Aldrich, 324558, 99.8%), and Acetone (C_3H_6O, Honeywell, 10626710) were all purchased and used without further purification.

AgNW characterization

A Scanning Electron Microscope (SEM) (FEI Quanta 600 field-emission gun with Bruker EDS X-ray microanalysis system and HKL EBSD system) at the Oklahoma State University Microscopy Lab was used to characterize the samples. To prepare the samples for SEM, stored samples were sonicated to fully disperse the AgNWs into solution. After sonication, the solutions were diluted 5 times with DI water. After dilution, 100 µL of AgNWs was pipetted onto carbon tabs adhered to aluminum pins. The samples were dried for 24 h under ambient conditions. Three SEM images were taken for each DoE reaction and were then analyzed by manually counting the number of wires and particles each image contained. Once each image was analyzed, a yield

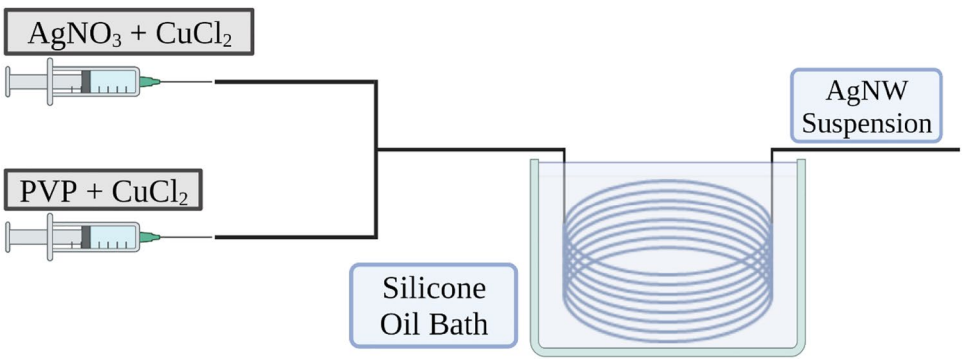

Fig. 12 A typical polyol AgNW MFR setup includes coiled tubing submerged in a silicone oil bath heated to reaction temperature, a syringe pump that controls reagent addition, reagents in syringes, and suspension collection at the outlet of the reactor (image created with BioRender)

of AgNWs was calculated for each image by dividing the counted number of AgNWs by the total number of wires and particles in that image. The three AgNW yields were then averaged to obtain a final average yield of AgNWs. After the final yield of AgNWs was obtained for each DoE reaction, the data were input to and analyzed by the Minitab software.

[AgNW] calculations

To calculate the concentration of AgNWs ([AgNWs])], a clean aluminum pin was weighed three times to obtain an average weight. AgNWs were sonicated to fully disperse the AgNWs into solution and then mixed on a stir plate. After the average weight was established, 100 µL of the AgNW solution was pipetted onto the aluminum pin and allowed to dry for 24 h under ambient conditions. This process was conducted a total of three times for one sample. To obtain an average [AgNW] in mg/mL, the pins are each weighed three times after fully dry and the difference between the clean pin weight and the dried weight is recorded. After dividing the average weight by the volume of the sample, an average [AgNW] value was obtained.

Conclusions

In this study, an optimized millifluidic polyol synthesis of AgNWs overcame the waste, reproducibility, distribution of size and morphology, and scalability issues associated with batch polyol AgNW reactions through control of a uniform chemical and thermal environment in a small segment of the reaction volume. A central composite, response surface, design of experiments was created to optimize the polyol reaction conditions to maximize the yield of AgNWs produced in a continuous, MFR. Based on the result of the design of experiments, the optimal reaction conditions are $T = 170$ °C, $[AgNO_3] = 0.177$ M, $[CuCl_2] = 6.05$ mM, and $[PVP] = 0.224$ M. The Minitab model predicted the yield of AgNWs with 85% accuracy while the DT and RF ML algorithms predicted the yield of AgNWs with 96.9% and 97.5% accuracy, respectively. Two separate optimized reactions reliably re-produced 100% AgNWs with average concentrations of 16 mg/mL (compared to 5 mg/m in millifluidic at optimized batch reaction conditions), lengths of 32 µm ($\sigma \pm 3.5$ µm), diameters of 68 nm ($\sigma \pm 12$ nm), and aspect ratios of 475. We also demonstrated the superiority of ML algorithms over linear regression models for predicting AgNWs yield. The proposed high-throughput MFR with the improved and optimized synthesis procedures along with ML models provide a platform for metal nanostructure manufacturing in which there is a systematic exchange between experiments and data-driven models. Discovery of an optimized, controllable, predictable, scalable, and low-cost manufacturing technology would be a major benefit to boost the manufacturing. Future work includes continuous chemically stabilizing AgNWs synthesized in a MFR at optimized reaction condition to further increase their stability against oxidation for nanoelectronics applications.

Acknowledgements This work was supported by the National Science Foundation (NSF) (Grant Agreement No.1939018).

Data Availability The supporting data for the conclusions drawn in this study can be obtained upon request from the corresponding author.

Declarations

Conflict of interest The authors have no competing interests to declare that are relevant to the content of this article.

References

Bamidele A, Emmanuel AO, Ijaola MB, Ajiteru O, Oyibo AM, Makhatha E, Asmatulu E (2022) Discovery and prediction capabilities in metal-based nanomaterials: an overview of the application of machine learning techniques and some recent advances. Adv Eng Inform 52:101593

Bertuit E, Neveu S, Abou-Hassan A (2022) High temperature continuous flow syntheses of iron oxide nanoflowers using the polyol route in a multi-parametric millifluidic device. Nanomaterials 12:119

Cao L, Huang Q, Cui J, Lin H, Li W, Lin Z, Zhang P (2020) Rapid and facile synthesis of high-performance silver nanowires by a halide-mediated, modified polyol method for transparent conductive films. Nanomaterials 10:1139

Chen D, Qiao X, Qiu X, Chen J, Jiang R (2011) Large-scale synthesis of silver nanowires via a solvothermal method. J Mater Sci Mater Electron 22:6–13

Choi S, Park J, Hyun W, Kim J, Kim J, Lee YB, Song C, Hwang HJ, Kim JH, Hyeon T, Kim D-H (2015) Stretchable heater using ligand-exchanged silver nanowire nanocomposite for wearable articular thermotherapy. ACS Nano 9:6626–6633

Coskun S, Aksoy B, Unalan HE (2011) Polyol synthesis of silver nanowires: an extensive parametric study. Cryst Growth Des 11:4963–4969

Dalchiele EA, Marotti RE, Cortes A, Riveros G, Gómez H, Martínez L, Romero R, Leinen D, Martin F, Ramos-Barrado JR (2007) Silver nanowires electrodeposited into nanoporous templates: Study of the influence of sizes on crystallinity and structural properties. Physica E 37:184–188

Galvão TLP, Novell-Leruth G, Kuznetsova A, Tedim J, Gomes JRB (2020) Elucidating structure-property relationships in aluminum alloy corrosion inhibitors by machine learning. J Phys Chem C 124:5624–5635

Gholizadeh M, Jamei M, Ahmadianfar I, Pourrajab R (2020) Prediction of nanofluids viscosity using random forest (RF) approach. Chemom Intell Lab Syst 201:104010

Gottesman R, Tangy A, Oussadon I, Zitoun D (2012) Silver nanowires and nanoparticles from a millifluidic reactor: application to metal assisted silicon etching. New J Chem 36:2456–2459
Han Yu, Tang B, Wang L, Bao H, Yuhao Lu, Guan C, Zhang L, Le M, Liu Z, Minghong Wu (2020) Machine-learning-driven synthesis of carbon dots with enhanced quantum yields. ACS Nano 14:14761–14768
Hemmati S, Barkey DP (2017) "Parametric study, sensitivity analysis, and optimization of polyol synthesis of silver nanowires",. ECS J Solid State Sci Technol 6:P132–P137
Hemmati S, Barkey DP, Gupta N, Banfield R (2015) Synthesis and characterization of silver nanowire suspensions for printable conductive media. ECS J Solid State Sci Technol 4:P3075–P3079
Hemmati S, Barkey DP, Gupta N (2016) Rheological behavior of silver nanowire conductive inks during screen printing. J Nanopart Res 18:249
Hemmati S, Barkey DP, Eggleston L, Zukas B, Gupta N, Harris M (2017) Silver nanowire synthesis in a continuous millifluidic reactor. ECS J Solid State Sci Technol 6:P144–P149
Hong C-H, Seung Kyu Oh, Kim TK, Cha Y-J, Kwak JS, Shin J-H, Byeong-Kwon Ju, Cheong W-S (2015) Electron beam irradiated silver nanowires for a highly transparent heater. Sci Rep 5:17716
Huang Q, Zhu Y (2019) Printing conductive nanomaterials for flexible and stretchable electronics: a review of materials, processes, and applications. Adv Mater Technol 4:1800546
Ji Z, Guo W, Wood EL, Liu J, Sakkiah S, Xiaoming Xu, Patterson TA, Hong H (2022) Machine learning models for predicting cytotoxicity of nanomaterials. Chem Res Toxicol 35:125–139
Kenry. (2023) Machine learning-assisted clustering of nanoparticle-binding peptides and prediction of their properties. Adv Theory Simul 6:2300122
Kinhal V, Krishna NB, Subramaniam P (2019) Transport and kinetic effects on the morphology of silver nanoparticles in a millifluidic system. Ind Eng Chem Res 58:5820–5829
Korte KE, Skrabalak SE, Xia Y (2008) Rapid synthesis of silver nanowires through a CuCl- or CuCl2-mediated polyol process. J Mater Chem 18:437–441
Kostowskyj MA, Gilliam RJ, Kirk DW, Thorpe SJ (2008) Silver nanowire catalysts for alkaline fuel cells. Int J Hydrogen Energy 33:5773–5778
Kumar A, Shaikh MO, Chuang C-H (2021) Silver Nanowire synthesis and strategies for fabricating transparent conducting electrodes. Nanomaterials 11:693
Kwon J, Suh YD, Lee J, Lee P, Han S, Hong S, Yeo J, Lee H, Ko SH (2018) Recent progress in silver nanowire based flexible/wearable optoelectronics. J Mater Chem C 6:7445–7461
Lau S, Kam SX, Chin ST, Tan FS, Lim WS, Chang CC, Yap MH, Jumali Hj, Zakaria S, Chook SW, Chia CH (2019) Silver nanowires as flexible transparent electrode: Role of PVP chain length. J Alloy Compd 803:165–171
Lee H, Kim M, Kim I, Lee H (2016) Flexible and stretchable optoelectronic devices using silver nanowires and graphene. Adv Mater 28:4541–4548
Li Y, Liu Y, Luo S, Wang Zi, Wang Ke, Huang Z, Zhao H, Jiang L (2020) Neural network model for correlating microstructural features and hardness properties of nickel-based superalloys. J Market Res 9:14467–14477
Liang J, Li Lu, Tong K, Ren Z, Wei Hu, Niu X, Chen Y, Pei Q (2014) Silver nanowire percolation network soldered with graphene oxide at room temperature and its application for fully stretchable polymer light-emitting diodes. ACS Nano 8:1590–1600
Liang X, Zhao T, Jiang W, Xuecheng Yu, Yougen Hu, Zhu P, Zheng H, Sun R, Wong C-P (2019) Highly transparent triboelectric nanogenerator utilizing in-situ chemically welded silver nanowire network as electrode for mechanical energy harvesting and body motion monitoring. Nano Energy 59:508–516
Liu L, Zhang Z, Cao L, Xiong Z, Tang Y, Pan Y (2021) Cytotoxicity of phytosynthesized silver nanoparticles:a meta-analysis by machine learning algorithms. Sustain Chem Pharm 21:100425
Luu QN, Doorn JM, Berry MT, Jiang C, Lin C, Stanley May P (2011) Preparation and optical properties of silver nanowires and silver-nanowire thin films. J Colloid Interface Sci 356:151–158
Lv H, Chen X (2022) Intelligent control of nanoparticle synthesis through machine learning. Nanoscale 14:6688–6708
Mahalle G, Salunke O, Kotkunde N, Gupta AK, Singh SK (2019) Neural network modeling for anisotropic mechanical properties and work hardening behavior of Inconel 718 alloy at elevated temperatures. J Market Res 8:2130–2140
Malandrino G, Finocchiaro ST, Fragalà IL (2004) Silver nanowires by a sonoself-reduction template process. J Mater Chem 14:2726–2728
Miller MS, O'Kane JC, Adrian Niec R, Carmichael S, Carmichael TB (2013) Silver nanowire/optical adhesive coatings as transparent electrodes for flexible electronics. ACS Appl Mater Interfac 5:10165–10172
Nathanael K, Cheng S, Kovalchuk NM, Arcucci R, Simmons MJH (2023) Optimization of microfluidic synthesis of silver nanoparticles: A generic approach using machine learning. Chem Eng Res Des 193:65–74
Nekahi A, Marashi SPH, Haghshenas Fatmesari D (2016) High yield polyol synthesis of round- and sharp-end silver nanowires with high aspect ratio. Mater Chem Phys 184:130–137
Ono T, Takebayashi Y, Kashiwagi T, Sue K (2023) Data-driven optimization of Au nanoparticle synthesis with automated flow microreaction system. J Chem Eng Jpn 56:2211125
Pareek A, Zafar M, Lakshminarayanan R, Joshi SJ (2021) Nanotechnology for green applications: how far on the anvil of machine learning! In: Joshi SJ, Prasad R, Jampilek J (eds) Nanotechnology for green applications. Springer International Publishing, Cham, pp 1–38
Roberts EJ, Karadaghi LR, Wang Lu, Malmstadt N, Brutchey RL (2019) Continuous flow methods of fabricating catalytically active metal nanoparticles. ACS Appl Mater Interfaces 11:27479–27502
Saraee S, Hossein HT, Jafarmadar S (2017) Experimental and numerical consideration of the effect of CeO2 nanoparticles on diesel engine performance and exhaust emission with the aid of artificial neural network. Appl Therm Eng 113:663–672
Sun Y, Mayers B, Herricks T, Xia Y (2003) Polyol synthesis of uniform silver nanowires: a plausible growth mechanism and the supporting evidence. Nano Lett 3:955–960
Support, Minitab 21. 2022a. 'Overview for Create Response Surface Design (Box-Behnken)', Minitab. https://support.minitab.com/en-us/minitab/21/help-and-how-to/statistical-modeling/doe/how-to/response-surface/create-response-surface-design/create-box-behnken-design/before-you-start/overview/.
Support, Minitab 21. 2022b. 'Summary of central composite designs'. https://support.minitab.com/en-us/minitab/21/help-and-how-to/statistical-modeling/doe/supporting-topics/response-surface-designs/summary-of-central-composite-designs/.
Tashkhourian J, Hormozi-Nezhad MR, Khodaveisi J (2011) Application of silver nanoparticles and principal component-artificial neural network models for simultaneous determination of levodopa and benserazide hydrochloride by a kinetic spectrophotometric method. Spectrochim Acta Part A Mol Biomol Spectrosc 82:25–30

Venkata Krishna Rao R, Venkata AK, Karthik PS, Singh SP (2015) Conductive silver inks and their applications in printed and flexible electronics'. RSC Adv 5:77760–77790

Xu J, Jun Hu, Peng C, Liu H, Ying Hu (2006) A simple approach to the synthesis of silver nanowires by hydrothermal process in the presence of gemini surfactant. J Colloid Interface Sci 298:689–693

Zhang P, Wyman I, Jiwen Hu, Lin S, Zhong Z, Yuanyuan Tu, Huang Z, Wei Y (2017) Silver nanowires: Synthesis technologies, growth mechanism and multifunctional applications. Mater Sci Eng, B 223:1–23

Zhao S, Wang Q, Zhaoming Qu (2018) Controlled synthesis of uniform silver nanowires via a simple polyol process. IOP Conf Ser Mater Sci Eng 301:012014

Zou G, Li H, Zhang Y, Xiong K, Qian Y (2006) Solvothermal/hydrothermal route to semiconductor nanowires. Nanotechnology 17:S313–S320